Journal of Membrane Science 369 (2011) 119–129

Contents lists available at ScienceDirect

Journal of Membrane Science

journal homepage: www.elsevier.com/locate/memsci

An experimental and theoretical analysis of molecular separations by diffusion through ultrathin nanoporous membranes

J.L. Snyder[a], A. Clark Jr.[b], D.Z. Fang[c], T.R. Gaborski[d], C.C. Striemer[c,d], P.M. Fauchet[c], J.L. McGrath[e,*]

[a] Department of Biochemistry and Biophysics, University of Rochester, 601 Elmwood Avenue, Box 712, Rochester, NY 14642, United States
[b] Department of Mechanical Engineering, University of Rochester, Rochester, NY 14627, United States
[c] Department of Electrical and Computer Engineering, University of Rochester, Rochester, NY 14627, United States
[d] SiMPore, Inc, 150 Lucius Gordon Dr., Suite 100, West Henrietta, NY 14586, United States
[e] Department of Biomedical Engineering, University of Rochester, Rochester, NY 14627, United States

ARTICLE INFO

Article history:
Received 3 June 2010
Received in revised form
18 November 2010
Accepted 23 November 2010
Available online 30 November 2010

Keywords:
Porous nanocrystalline silicon
Nanoporous membrane
Diffusion
Separation
Modeling

ABSTRACT

Diffusion based separations are essential for laboratory and clinical dialysis processes. New molecularly thin nanoporous membranes may improve the rate and quality of separations achievable by these processes. In this work we have performed protein and small molecule separations with 15 nm thick porous nanocrystalline silicon (pnc-Si) membranes and compared the results to 1- and 3-dimensional models of diffusion through ultrathin membranes. The models predict the amount of resistance contributed by the membrane by using pore characteristics obtained by direct inspection of pnc-Si membranes in transmission electron micrographs. The theoretical results indicate that molecularly thin membranes are expected to enable higher resolution separations at times before equilibrium compared to thicker membranes with the same pore diameters and porosities. We also explored the impact of experimental parameters such as porosity, pore distribution, diffusion time, and chamber size on the sieving characteristics. Experimental results are found to be in good agreement with the theory, and ultrathin membranes are shown to impart little overall resistance to the diffusion of molecules smaller than the physical pore size cutoff. The largest molecules tested experience more hindrance than expected from simulations indicating that factors not incorporated in the models, such as molecule shape, electrostatic repulsion, and adsorption to pore walls, are likely important.

1. Introduction

Membranes with nanometer scale pores are an important technology for the separation of proteins and small molecules, with use in research, industrial, and clinical arenas. Dialysis, a diffusion based separation modality requiring a nanoporous membrane, is a staple in laboratory purifications and buffer exchanges. Similarly, the clinical process of hemodialysis utilizes nanoporous membranes for the diffusive separation of proteins coupled with pressurized flow for fluid balance. The development of new membrane materials is needed to improve the precision and efficiency of these frequently used procedures [1,2].

Many of the polymer based membranes currently used in dialysis have long tortuous pores and log normal pore distributions with extended tails [3], resulting in low resolution molecular weight cutoffs. With pore characteristics such as these, only molecules differing significantly in size can be clearly separated. This is of significant concern in hemodialysis. Low-flux dialysis membranes are able to filter urea and small toxins while retaining serum albumin, but often unwanted middle weight molecules, including β_2-microglobulin, cytokines, and leptin, are retained as well [4]. Retention of β_2-microglobulin in particular can cause amyloidosis and can be used as a predictor of patient mortality [5,6]. High-flux membranes, which have larger pore sizes and cutoffs, are able to better clear middle weight species, but have been linked to serum albumin loss [7,8].

In addition to having non-ideal pore distributions, traditional dialysis membranes are orders of magnitude thicker than their nominal pore size. The diffusion of molecules traversing this thickness is greatly reduced compared to free diffusion, requiring long times for laboratory and clinical separations. This has lead to a call for thin nanoengineered membranes to enable wearable dialysis units [9]. In the case where filters are used for isolating small analytes, the thickness and tortuous pores present high surface area for adsorption, which may result in the significant loss of low abundance species.

Due to the infrastructure created by the microelectronics industry, silicon is an attractive fabrication platform for engineered nanomembranes [10]. Silicon based membranes with arrays of well

Abbreviations: pnc-Si, porous nanocrystalline silicon.

* Corresponding author. Tel.: +1 585 2735489; fax: +1 585 2761999.
E-mail address: jmcgrath@bme.rochester.edu (J.L. McGrath).

0376-7388/$ – see front matter © 2010 Elsevier B.V. All rights reserved.
doi:10.1016/j.memsci.2010.11.056

defined slit pores fabricated via photolithography techniques have been shown to be useful in a number of separation and biological experiments [11]. Silicon has also been used as a platform for aligned carbon nanotube (CNT) growth and the creation of CNT membranes [12,13]. However, both of these novel membranes are still many microns thick. In 2004, Tong et al. fabricated an ultrathin (10 nm) silicon nitride nanosieve with precise, individually drilled pores, a process that is too time consuming for scale up [14]. More recently, a thin (0.7–1 μm) anodized alumina membrane, in which the pores self-assemble, was developed with the use of thin film deposition on silicon, although the pore sizes 0.7–1 μm are not on the same scale as the nanosieve [15].

We have previously reported an ultrathin porous membrane material with self-assembling pores called porous nanocrystalline silicon (pnc-Si) [16]. Previous studies with these membranes have shown diffusion based separations of binary mixtures of proteins [16] and the rapid diffusion of small molecules through the pores [17]. In addition, recent experiments have shown that pnc-Si has high hydraulic permeability [18], can precisely separate closely sized nanoparticles under pressure [18], and can be used as a highly permeable cell culture substrate [19]. Pnc-Si membranes are fabricated using standard photolithography and silicon chip manufacturing techniques. The freestanding membranes can be made between 7 and 30 nm thick, which is on the same order as their pore sizes. Pore sizes can be tuned by adjusting annealing temperature or ramp rate during pnc-Si production, and pore distributions, which are directly measured using transmission electron microscopy [18], fall within the size scale of small molecules, proteins, and larger complexes. While pnc-Si membranes have a distribution of pores, the membranes have a distinctly sharp cutoff. Current processes enable the production of more than 100 membrane chips per 4 in. wafer, and this process can be scaled up to a 6 in., 8 in., or 12 in. substrate, which would enable the production of thousands of chips per wafer or whole wafer membrane cartridges for dialysis procedures.

Because of their thinness and unambiguous pore distributions, pnc-Si membranes can be used to test theories of molecular diffusion and can help in understanding how ultrathin membranes can impact diffusive separations. While a porous membrane will prevent any molecule larger than the largest pore from diffusing through, it also hinders the diffusion of molecules smaller than this pore size. Traditional theory suggests that the hindrance is due to (1) steric interactions between the molecule and the pore entrance and (2) frictional interactions between the molecule and the pore walls as it passes through [20]. This theory has seen experimental verification with experiments using track etched mica [21] and porous alumina membranes [22]. Early hindrance models considered the diffusion solely along the central axis of the pore [20,23,24], although newer treatments average the hindrance radially across the entire cross-section [25]. An additional cause of hindrance arises from the parallel diffusion of molecules across the membrane surface between pores [17,27]. The parallel diffusion and entrance effects are negligible for a thick membrane but significantly contribute to the total resistance of an ultrathin membrane; once a molecule finds a pore it needs only to diffuse a distance on the order of its own length to exit the other side.

In this work we have performed separations with proteins and small molecules using pnc-Si membranes. Using equations defining the resistance to diffusion along the surface of and through a membrane, we have developed 1-dimensional and 3-dimensional models of molecular diffusion. We used these models to analyze the influence of factors such as membrane thickness, porosity, pore size distribution, time of separations, and system geometry on separations. The experimental results were compared with the diffusion models, and good agreement was observed for small molecules.

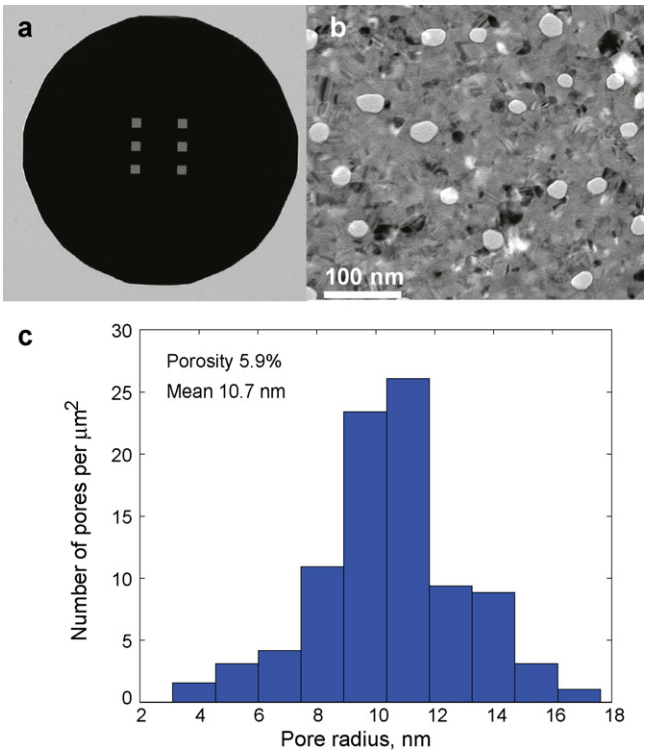

Fig. 1. Pnc-Si membrane. (a) 6.5 mm diameter silicon chip with six 0.2 mm × 0.2 mm freestanding pnc-Si membranes. (b) TEM micrograph of nanometer scale pores in 15 nm thick pnc-Si membrane film. Pores are white ellipsoids and nanocrystals are black spots. (c) Pore characteristics as determined from image processing of 2 μm squared area of micrograph.

We consider the effect of protein adsorption, and we discuss the potential effects of additional factors including molecular shape, electrostatics, and convection.

2. Experimental

2.1. Pnc-Si membrane fabrication and characterization

Detachable chips with 15 nm thick freestanding pnc-Si membranes were fabricated on 200 μm thick 4 in. silicon wafers according to Striemer et al. [16]. 6.5 mm diameter circular chips with six 0.2 mm × 0.2 mm windows of freestanding pnc-Si membranes were prepared for the experimental separations (Fig. 1a). Pore characterization was performed using transmission electron microscopy (TEM) on 3 mm diameter chips, which are smaller in diameter so as to fit into the TEM sample holder. Each TEM chip had four 0.1 mm × 0.1 mm windows of freestanding pnc-Si membranes. The wafers were annealed in a Solaris 150 rapid thermal processing unit (Surface Science Integration, El Mirage, AZ) at 1000 °C for 60 s with a ramp rate of 100 °C/s.

A Hitachi H-7650 transmission electron microscope was used to view the TEM formatted chips in bright-field mode at 80 kV. Micrographs were taken with an Olympus Cantega 11 megapixel digital camera at a resolution of 100 kX. The TEM micrograph in Fig. 1b shows white open pores and black diffracting nanocrystals within the gray crystallized film. Pore characteristics were determined from TEM micrographs using a MATLAB based image processing program developed by our group (available at: http://nanomembranes.org/resources/software/) (Fig. 1c). A trained operator can use the program to find pore edges and thereby determine the shape and dimensions of pores and the porosity [18].

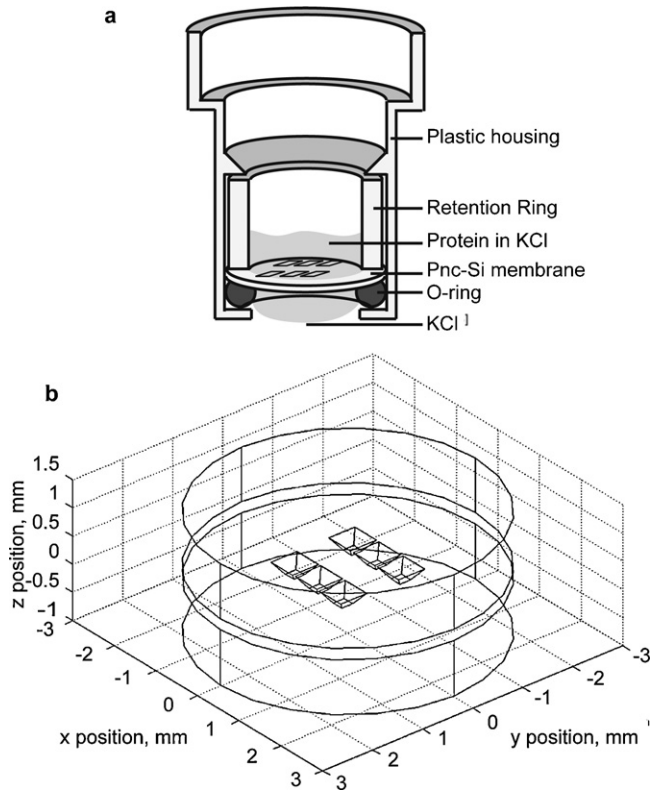

Fig. 2. Experimental setup and 3-D computational diffusion model. (a) Schematic of experimental setup. (b) CAD model of experimental system: 6 windows covered with 15 nm thick membrane material separate two fluid wells.

2.2. Protein and small molecule separations

We set up an experimental system that enabled the separations of several proteins and small molecules. The experimental chips from Section 2.1 were sealed into polypropylene SepCon tubes (SiMPore Inc., West Henrietta, NY) between a viton o-ring and a polypropylene retention ring (Fig. 2a). The polypropylene tube held the fluid wells in contact with the ultrathin membrane, and the retentate and dialysate were removed at the completion of the diffusion experiment.

A series of differently sized proteins and small molecules were prepared for separation experiments. β-galactosidase, phosphorylase b, bovine serum albumin, ovalbumin, and carbonic anhydrase (Sigma–Aldrich, St. Louis, MO) were dissolved 100 mM KCl at a 1 mg/mL concentration. Myosin (Sigma) was used as an intact membrane control, as it is too large to pass through the nanopores. Rhodamine 6 g and hydrogen peroxide were prepared at 100 μM in 100 mM KCl. For each protein or small molecule being tested, 20 μL of the sample was pipetted onto the retentate side of the membrane and 20 μL of 100 mM KCl was pipetted onto the dialysate side. Membranes selected for the experiments had pore characteristics as indicated in Fig. 1c (Porosity 5.9%, Mean pore radius 10.7 nm). Diffusion was allowed to occur for 24 and 48 h time points in a sealed container to prevent evaporation.

The retentate and dialysate samples were collected at the completion of the experiment. The protein samples were analyzed using SDS polyacrilamide gel electrophoresis (SDS-PAGE). The hydrogen peroxide was measured using the Amplex Red hydrogen peroxide kit (Invitrogen, Carlsbad, CA) which produces a colored substrate. Absorbance scans of cytochrome c, rhodamine 6 g, and Amplex Red assay were taken using an Infinite M200 plate reader (Tecan, Mannedorf, Switzerland). The dimensions of the proteins and small molecules were obtained from literature and from dynamic light scattering measurements using a Zetasizer (Malvern, Worchestershire, UK).

3. Theory

3.1. 1-D analytical model

To understand dialytic separations with ultrathin membranes, we first developed a simple 1-dimensional model comprised of two fluid wells of length a, separated by a membrane with thickness d (Fig. 5a). The retentate well, so named as it will contain molecules retained by the membrane at the completion of the simulation, is given an initial homogeneous concentration of molecules. Over the course of the simulation, molecules able to diffuse through the pores will enter the dialysate well. The diffusion of species is governed by Fick's Second Law of diffusion,

$$\frac{\partial c}{\partial t} = D\frac{\partial^2 c}{\partial x^2}, \tag{1}$$

where c is the concentration, t the time, D the diffusion coefficient, and x the position within the model. In each fluid well, the diffusing species have a free diffusion coefficient as defined by the Stokes–Einstein relation,

$$D_0 = \frac{kT}{6\pi\eta R_s}, \tag{2}$$

where k is Boltzmann's constant, T the temperature, η the viscosity, and R_s the molecule radius. Diffusion through the membrane is characterized with a reduced diffusion coefficient D_m, where D_m is a function of both molecule and pore sizes (see below).

As the fluid wells are several orders of magnitude longer than the membrane is thick, we can assume the membrane is in a quasi-steady state and that the concentration profile in this region is linear [28]. This means that at a point x within the membrane, the concentration will be given by

$$c(x,t) = c(a,t) - (x-a)\frac{c(a,t) - c(a+d,t)}{d}. \tag{3}$$

The flux within the membrane, F_m can then be written as

$$F_m = -D_m\frac{\partial c}{\partial x} = D_m\frac{c(a,t) - c(a+d,t)}{d}. \tag{4}$$

If we neglect molecular adsorption to the membrane, the flux within the membrane, Eq. (4), is equal to the flux entering from or leaving the membrane to the fluid wells, F_f,

$$F_f = -D_0\frac{\partial c}{\partial x}\bigg|_{x=a} = -D_0\frac{\partial c}{\partial x}\bigg|_{x=a+d} = F_m. \tag{5}$$

We use Eqs. (3)–(5) to form the following jump condition describing the change in concentration across the membrane,

$$c(a+d,t) - c(a,t) = -\frac{F_f d}{D_m} = \frac{D_0 d}{D_m}\frac{\partial c}{\partial x}. \tag{6}$$

We will treat the membrane at position a as an infinitely thin discontinuity in concentration, although the membrane thickness d is necessary in the calculation of the concentration jump condition.

To develop a non-dimensional statement of diffusion between the two compartments, we first introduce the parameter β,

$$\beta = \frac{D_0 d}{D_m a}, \tag{7}$$

as a ratio of membrane resistance, Ω_m to well resistance, Ω_w, or

$$\beta = \frac{d/D_m}{a/D_0} = \frac{\Omega_m}{\Omega_w}. \tag{8}$$

We also introduce the following scaled forms of our variables:

$$\hat{x} = \frac{x}{a}, \quad \hat{t} = \frac{tD_0}{a^2}, \quad \hat{c} = \frac{c - C_2}{C_1 - C_2}, \tag{9}$$

where C_1 is the initial concentration of the molecule to be simulated in the retentate and C_2 the initial concentration in the dialysate. The final non-dimensional problem is:

$$\frac{\partial \hat{c}}{\partial \hat{t}} = \frac{\partial^2 \hat{c}}{\partial \hat{x}^2}, \quad 0 \le \hat{x} < 1 \text{ and } 1 < \hat{x} \le 2, \tag{10}$$

$$\frac{\partial \hat{c}}{\partial \hat{x}}(0, \hat{t}) = 0, \quad \frac{\partial \hat{c}}{\partial \hat{x}}(2, \hat{t}) = 0, \tag{11}$$

$$\hat{c}(1+, \hat{t}) - \hat{c}(1-, \hat{t}) = \beta \frac{\partial \hat{c}}{\partial \hat{x}}(1\pm, \hat{t}), \tag{12}$$

$$\frac{\partial \hat{c}}{\partial \hat{t}}(1+, \hat{t}) - \frac{\partial \hat{c}}{\partial \hat{t}}(1-, \hat{t}) = 0, \tag{13}$$

$$\hat{c}(\hat{x}, 0) = \begin{cases} 1 & 0 \le \hat{x} < 1, \\ 0 & 1 < \hat{x} \le 2. \end{cases} \tag{14}$$

Eq. (10) is a dimensionless statement of Fick's Second Law, which holds for the entire system except for the discontinuity at the membrane. Eq. (11) represents the requirement for no outward flux at the walls. Eq. (12) is a non-dimensional form of Eq. (6) that incorporates the idea of a discontinuity at the membrane. Eq. (13) ensures the continuity of flux entering and leaving the membrane within the fluid well portion of the model. Eq. (14) is the initial concentration condition, which give the retentate and dialysate non-dimensional concentrations of 1 and 0 respectively.

The solution to this problem is (see Appendix A):

$$\hat{c}(\hat{x}, \hat{t}) = \frac{1}{2} + \sum_{n=1}^{\infty} \frac{\sin \lambda_n}{\lambda_n + \cos \lambda_n \sin \lambda_n} \psi_n(\hat{x}) e^{-\lambda_n^2 \hat{t}}, \tag{15}$$

where the eigenfunctions ψ_n are given by

$$\psi_n(\hat{x}) = \begin{cases} \cos \lambda_n \hat{x} & 0 \le \hat{x} < 1, \\ -\cos \lambda_n (2 - \hat{x}) & 1 < \hat{x} \le 2, \end{cases} \tag{16}$$

and the eigenvalues λ_n are found by solving the following transcendental equation,

$$\tan \lambda_n = \frac{2}{\beta \lambda_n}. \tag{17}$$

For comparison purposes, we have also found an analytic solution for diffusion in an identical system lacking a membrane (Appendix B).

3.2. Defining membrane resistance

Membrane characteristics, including thickness, porosity, and pore distribution, can be directly incorporated into the analytical solution through the parameter β. In this manner, we can test the resistance imparted by specific membranes on a range of molecule sizes. We will consider the membrane resistance to be from two sources: (1) pore discovery via diffusion to the pore entrance [17,29] and (2) the steric and frictional hindrance as a molecule enters and passes through a pore [20,23–25].

It has been shown that small molecules encounter negligible hindrance as they diffuse across an ultrathin membrane [17]. The limiting factor for the permeation of these molecules is locating and diffusing to a pore, as pore to pore distances are often greater than the membrane thickness. By modifying an expression for the trapping rate of molecules to an adsorbing patch on a surface [29], Kim et al. developed a simple expression for the permeability, κ, of a small molecule through a membrane,

$$\kappa = 2D_0 N R_P, \tag{18}$$

where N is the density of pores and R_p is the average pore radius [17]. As this expression neglects steric or frictional hindrances within the pore, we can consider it to be a statement of the pore discovery permeability, P_d. We can rewrite Eq. (18) given the pore distributions of pnc-Si membranes as

$$P_d = \frac{2D_0}{A} \sum_i R_{pi}, \tag{19}$$

where i is the index over every pore in the distribution as determined by TEM image processing, A the processed area of the TEM images, and R_p the particular pore radius.

As the size of the molecule increases relative to the pore sizes, so do the effects of steric and frictional hindrance. We use a cross sectionally averaged hindrance equation to determine the reduced diffusion coefficient D_m,

$$\frac{D_m}{D_0} = 1 + \frac{9}{8}\xi \ln \xi - 1.56034\xi + 0.528155\xi^2 + 1.91521\xi^3 - 2.81903\xi^4 + 0.270788\xi^5 + 1.1015\xi^6 - 0.435933\xi^7, \tag{20}$$

where ξ is the ratio of molecule radius to pore radius (R_s/R_p) [25]. We can determine the transmembrane permeability, P_t, by summing the diffusion coefficients weighed by the contribution of each pore to the porosity,

$$P_t = \frac{1}{Ad} \sum_i D_{mi} \pi R_{pi}^2. \tag{21}$$

Both the pore discovery and the transmembrane permeabilities are functions of the molecule size and membrane characteristics and are independent of the concentration difference.

The membrane resistance, Ω_m, or reciprocal of the total permeability, can be obtained by adding the permeabilities like conductances in series [26],

$$\Omega_m = \frac{1}{(1/P_d) + (1/P_t)}. \tag{22}$$

The membrane resistance can then be inserted into Eq. (7) to obtain the ratio of resistances β.

3.3. 3-D computational model

While the 1-D analytic model provides the most basic description of diffusion through an ultrathin membrane and allows simple analysis of the physics of this process, it is not readily comparable with our experiments due to the 3-D geometry of our device. To make this comparison, we have created a 3-dimensional model using the transient diffusion module of COMSOL Multiphysics (COMSOL, Stockholm, SWE). A CAD representation consistent with our experimental system, retentate and dialysate wells separated by a membrane of specific thickness and active area, was built in COMSOL (Fig. 2b). Simulated molecules were given diffusion coefficients according to Eq. (2). We determined the total permeability of the membrane from pore distributions, Eq. (22), and multiplied it by the membrane thickness to obtain a membrane diffusion coefficient.

The model was meshed by creating a swept mesh through the membrane region by connecting "Extremely Fine" predefined meshes in the wells. The larger fluid wells were then re-meshed with a "Finer" predefined mesh. An initial concentration was specified for the retentate well at time 0, and diffusion was simulated for 24 and 48 h. The concentration of the molecule tested was integrated throughout the retentate and dialysate wells, and a ratio was taken to obtain the sieving coefficients, Eq. (23). Batch processing for multiple molecules was performed using MATLAB (The MathWorks, Natick, MA).

4. Results and discussion

4.1. Protein and small molecule separations

In Fig. 3a we show representative SDS-PAGE results of a 24 h separation of myosin, β-galactosidase, phosphorylase b, albumin, ovalbumin, and carbonic anhydrase using pnc-Si membranes. The smaller proteins diffuse into the dialysate, while the largest remain within the retentate only. Mass balances show that little protein is adsorbed in this system, as the sum of retentate and dialysate band intensities add up to the starting solution (Fig. 3b). Adsorption in our system can occur on the plastic housing or surface of the membrane, but membrane internal area is low compared to conventional membranes (0.01 μm^2 instead of 100 μm^2 of internal surface area per μm^2 of frontal surface) [18]. We also obtained absorbance scans of retentate and dialysate wells for separations of colored species, as demonstrated for rhodamine 6 g in Fig 3c.

We use a ratio of dialyate to retentate concentrations,

$$S = \frac{c_{\text{dialysate}}}{c_{\text{retentate}}}, \tag{23}$$

to track the extent of molecular diffusion within the system. We refer to S as a sieving coefficient because of its similarity in definition and use to the sieving coefficient used in convective transport based separations [30]. While sieving coefficients are not normally used to describe diffusion based systems, we find that such a measure is of use in the visualization of separations in our experiments and model. At equilibrium, both dialysate and retenate would have the same concentration and S is equal to 1. Since intensity is proportional to concentration, we can determine S for the protein samples by taking a ratio of dialysate to retentate band intensities from the images of the SDS-PAGE gels using ImageJ [31]. S for colored species was taken as the ratio of peak absorbance of the dialysate to the retentate. In Fig. 3d we show sieving coefficients for a 24 h diffusion experiment plotted against sizes as obtained by literature and dynamic light scattering measurements (Table S3 in Supplement).

4.2. Resistance components

The diffusion models were used to better understand the factors, such as membrane resistance, which influence molecular passage in our experiments. In our models, we consider the membrane resistance to be the combination of two separate resistances, the pore discovery ($1/P_d$) and transmembrane ($1/P_t$) resistances. The characteristics of the membrane greatly affect the contributions of each of these terms. In Fig. 4a we show the pore discovery resistance, transmembrane resistance, and the sum of these resistances for a 15 nm thin membrane with the pore characteristics the pnc-Si membranes used in the experiments (Fig. 1c). In an ultrathin membrane, the pore discovery resistance is on the same order or sometimes greater than the transmembrane resistance for molecules much smaller than the physical pore cutoff. Steric and frictional hindrances within the membrane are minimal for small molecules, but since the distance between pores is similar to the distance through the pores, the pore discovery resistance can be significant and in some cases even dominant (see Supplement). For larger molecules, the transmembrane resistance outweighs the pore discovery resistance and eventually becomes infinite for molecules as large as or larger than the pores.

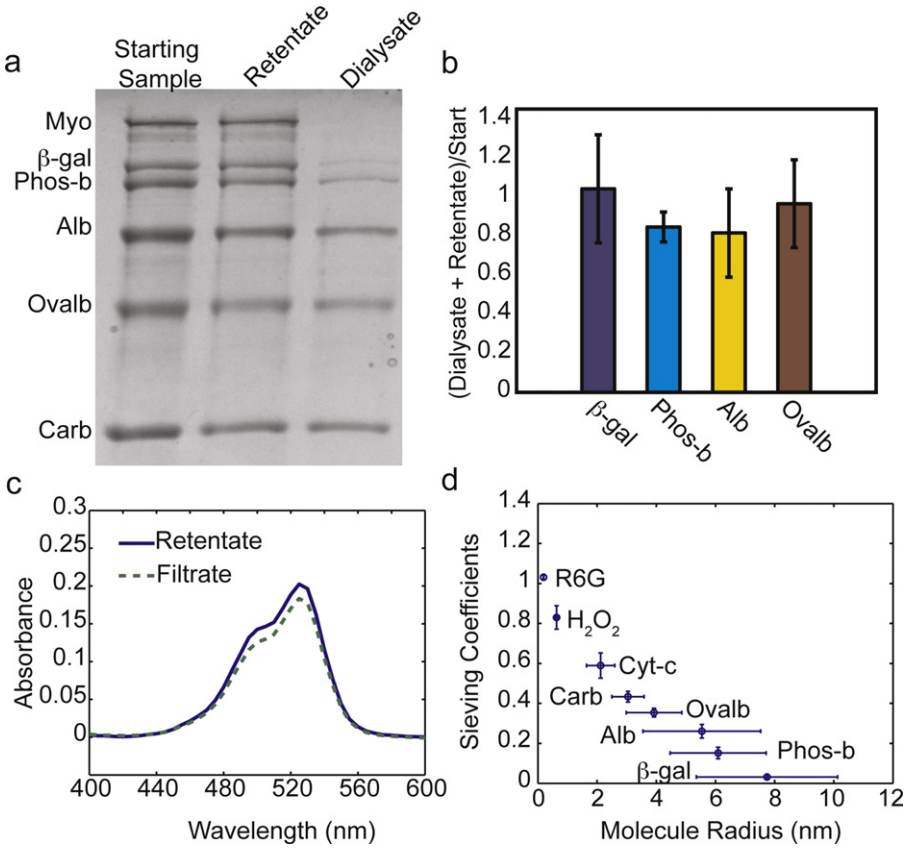

Fig. 3. Experimental Results. (a) SDS-PAGE of 24 h protein separation. As proteins get smaller in size, they diffuse through the membrane to a greater extent. Myosin serves as an intact membrane control. (b) Mass balance performed by normalizing retentate and dialysate SDS-PAGE gel band intensity to band intensity of starting sample. (c) Absorbance scans of rhodamine 6 g at 24 h. (d) Sieving coefficients from experimental proteins and small molecules for a 24 h separation with molecule sizes determined by DLS (Myo – myosin, β-gal – β-galactosidase, Phos-b – phosphorylase-b, Alb – albumin, Ovalb – ovalbumin, Carb – carbonic anhydrase, Cyt-c – cytochrome c, R6G – rhodamine 6 g).

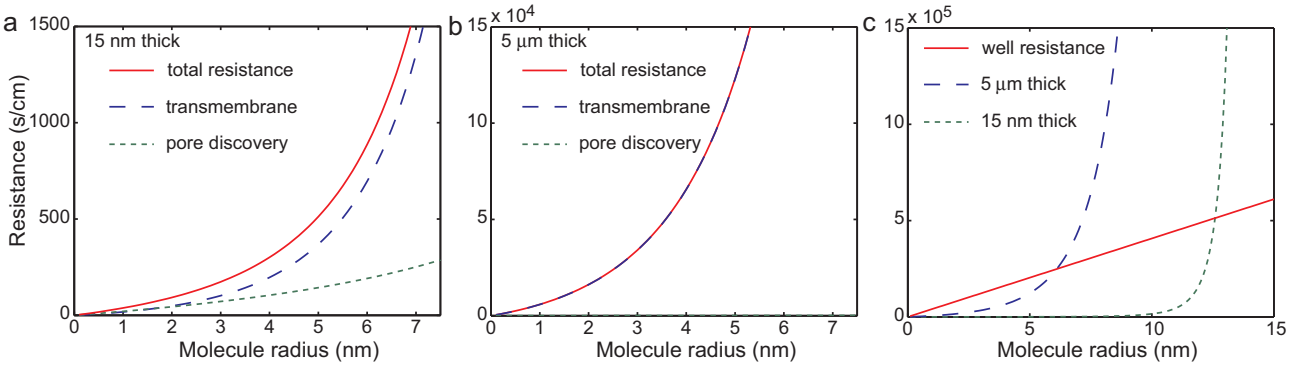

Fig. 4. Components of resistance for thin and thick membranes with 15 nm pores and comparison to fluid well resistance. (a) Resistances for an ultrathin (15 nm) membrane. For small molecules, the transmembrane and pore discovery resistances are similar. The addition of the two create a larger total resistance. At molecule sizes approaching the pore size, the transmembrane permeability dominates the total resistance. (b) Resistances for a thick (5 μm) membrane. Transmembrane resistance is the dominating resistance for all molecule sizes and overlaps with the total resistance in this panel. The pore discovery resistance has the same values as in panel a., though is too small in comparison to be viewed. (c) Comparison of well resistance and membrane resistance for thick and ultrathin membranes. Due to the high transmembrane resistance in thick membranes, the total membrane resistance surpasses the fluid well resistance at much smaller molecule sizes than the ultrathin membrane case.

In thick membranes with the same pore characteristics of a pnc-Si membrane, the transmembrane resistance dominates for all molecule sizes (Fig. 4b). The numerical value of the total resistance in thick membranes is also much higher than ultrathin membranes. A comparison can also be made between total membrane resistances and the resistance to diffusion within the fluid wells (Fig. 4c). The total resistance for thick membranes surpasses the well resistance at smaller molecule sizes than for ultrathin membrane, even though both membranes have the same pore radii and porosity.

4.3. Visualizing membrane resistance

The 1-D analytical model removes geometric complexity and reduces the problem to the basic physics of separation. This enables simple visualization and analysis of the theoretical separations. In Fig. 5 we compare results for the diffusion of a 5 nm radius molecule through no membrane, an ultrathin membrane (15 nm), and a thick membrane (5 μm). Both membranes were given pore distributions from the pnc-Si membrane in Fig. 1c. The separations depicted in Fig. 5 are for a system with 1 mm fluid wells at 0, 100, 1000, and 10,000 s.

The concentration profiles of the free diffusion (Fig. 5b) and ultrathin membrane (Fig. 5c) simulations are identical, indicating that a 5 nm radius molecule experiences neglible hindrance from the molecularly thin membrane under these conditions. While there is resistance from the ultrathin membrane, a molecule only experiences this hindrance over a distance similar to its own size, and so the transport time is negligible compared to bulk transport.

A 5 μm thick membrane with the same pore characteristics as the 15 nm thick membrane has a 300× larger β, Eq. (7), for a separation with a 5 nm radius molecule. The concentration profiles for this case (Fig. 5d) demonstrate an obvious concentration jump across the membrane. The higher resistance slows the diffusion of the molecules through the membrane and increases the time required for the system to reach equilibrium.

4.4. Sieving by thin and thick membranes

To visualize separations over an entire range of molecule sizes, we use the 1-D model to generate sieving coefficients, Eq. (23), over time. To simplify the analysis, we have used a monodisperse, 10 nm radius pore distribution. The sieving coefficients for molecule radii ranging from 0.5 to 12 nm and times of 1, 6, and 24 h using both 15 nm and 5 μm thick membranes are shown in Fig. 6. Again, we have included a free diffusion case for comparison. A sieving coefficient of 1 indicates that the system has reached equilibrium.

We observe that diffusion through ultrathin membranes follows the free diffusion curve until the molecule size is within ~30% of the physical pore cutoff for short times and ~10% for long times. The steepness of the sieving profile near the cutoff indicates that high resolution separations are possible with molecularly thin membranes and that the resolution improves as equilibrium is approached. In contrast, separations with thick membranes lag behind the free diffusion curves at all times. Even the diffusion of the smallest molecules through thick membranes is slowed by the 10 nm radius pores. The hindrance is higher for molecules in the thicker membrane because of the length of the pores they must diffuse through, and this would lower the resolution of a separation at any time point. Thus molecularly thin membranes are expected to fractionate mixtures based on size more quickly and with a higher resolution cutoff than their thick counterparts at all times before equilibrium.

4.5. Factors that influence membrane separations

In addition to membrane thickness, several other factors can affect the performance of membranes in dialysis, including (1) porosity, (2) pore size distributions, (3) time of separations, and (4) well geometry. Understanding the impact of these factors is important for the optimization of experimental separations. We can visualize the effect of these factors by normalizing sieving coefficients with membranes, S_{mem}, to those from a membraneless separation, S_0. The ratio S_{mem}/S_0 deviates from 1 as membrane resistance slows transport relative to free diffusion. A curve generated by taking this ratio for a range of molecule sizes will be referred to as a normalized sieving profile. In the panels of Fig. 7 we examine the effects of porosity (Fig. 7a), pore size distributions (Fig. 7b), time (Fig. 7c), and well geometry (Fig. 7d) on the normalized sieving profile. A dotted line indicates the projected equilibrium at infinitely long times.

We first investigated the influence of porosity on separations (Fig. 7a). The results show that as the porosity of an ultrathin membrane decreases, the effective cut-off and sieving resolution of the membrane both decrease at a particular time point. Recalling that the resolution improves as equilibrium is approached, we see that the lower porosity diminishes resolution by directly increasing both pore discovery and transmembrane resistances and slowing transport. A thick (5 μm) membrane with 5% porosity is shown for comparison. Note that even with 10× lower porosity than a thick membrane, an ultrathin membrane exhibits sharper resolution separations at the same time point.

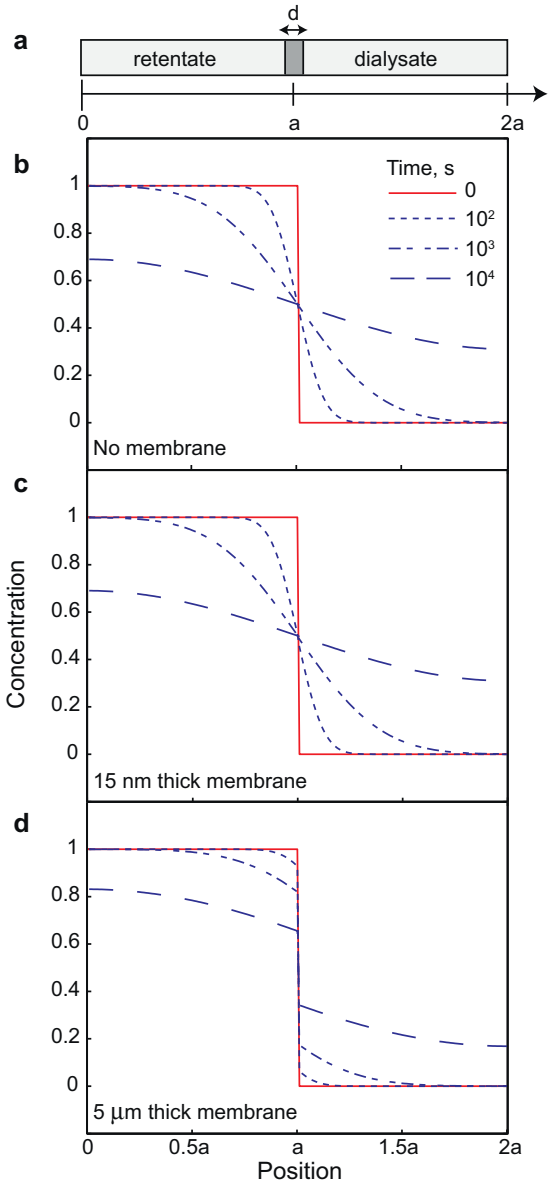

Fig. 5. Concentration profiles in 1-D model. (a) Schematic of 1-D analytic model: retentate and dialysate fluid wells are separated by a membrane of thickness *d*. (b) In a simulation without a membrane, a 5 nm radius molecule diffuses into the dialysate well ($a = 1$ mm) by free diffusion. (c) In the case of an ultrathin (15 nm thick) membrane, in which the 5 nm radius molecule is significantly smaller than the largest pores in the distribution (Fig. 1c), the diffusion is indistinguishable from the no membrane case. (d) If a thick (5 μm) membrane with the same pore radii and porosity separates the wells, the diffusion is hindered, as indicated by the large concentration jump across the membrane and the slower approach to equilibrium.

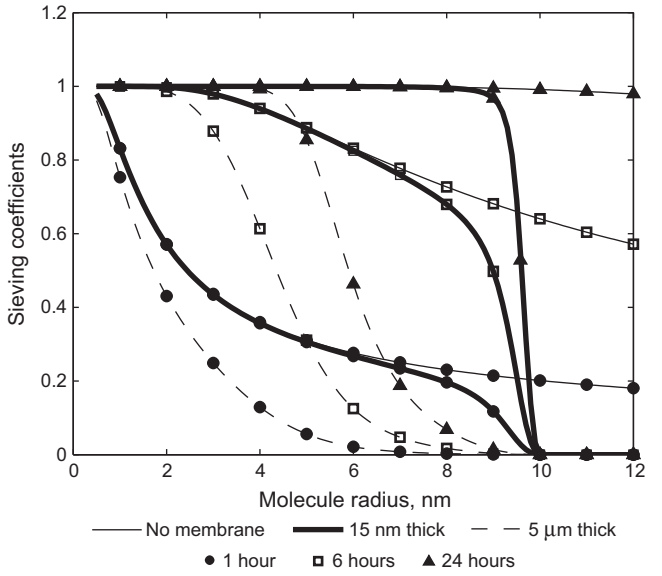

Fig. 6. Sieving profiles of 15 nm thick and 5 μm thick membranes for 1, 6, and 24 h time points. Both 15 nm and 5 μm thick membranes have a pore radius cutoff of 10 nm. A no membrane (free diffusion) simulation at each time point is shown for comparison. For small molecules, the diffusion through the thin membrane is indistinguishable from free diffusion. Diffusion through the thin membrane slows as the molecules approach the size of pore cutoff. The thick membrane shows strong hindrance at all molecule sizes, raising the time to equilibrium and lowering the resolution of the separation.

Next we inspected the contribution of different pore sizes on separations with ultrathin membranes (Fig. 7b). To perform this analysis, porosity was kept constant at 5%, and we simulated membranes with 5 nm radius pores (636 pores/μm^2) and 10 nm radius pores (159 pores/μm^2). The 10 nm radius pore membrane exhibits a sharp drop in the normalized sieving profile near the 10 nm cut-off, and a similar 5 nm cutoff is visible for the 5 nm radius pore membrane. If we add the pore distributions of these membranes together and simulate a 5 and 10 nm radius pore membrane with 10% porosity, we see a normalized sieving profile similar in appearance to the original 10 nm radius pore membrane. This illustrates that pores significantly below the physical pore cutoff do not contribute to the separation even through they increase the overall membrane porosity. In the case of the thick membrane, the addition of the 5 nm radius pores does effect the normalized sieving profile for the smallest molecules. Although the effect on the sieving profile is slight, it serves to illustrate that thicker membranes are more sensitive to pores below the cut-off than ultrathin membranes.

We then examined the effect of time on the normalized sieving profiles (Fig. 7c). As we saw for non-normalized sieving curves (Fig. 6), shorter times are associated with smaller effective cut-offs and lower resolution. This is because small size differences between molecules can result in significant hindrance differences at short times. The non-equilibrium profiles are not only relevant for short duration experiments, but they can represent the steady-state profiles in a device where a constant concentration jump is maintained across the membrane by the supply and removal of species. Our results suggest that diffusion in such a situation would deviate from free diffusion for molecules within ~30% of the pore size cut-off.

The final factor we have chosen to investigate is the geometry of the experimental system. Separations in longer fluid wells will have a larger equilibrium time constant, τ,

$$\tau = \frac{a^2}{D_0}, \tag{24}$$

and in Fig. 7d we show simulations at 0.4 τ for several geometries (Fig. 5d). Specifically, we compare our standard 1 mm well at 1 h to a 1 cm well at 100 h and a 50 μm well at 1/400th of an hour (9 s). Even though each system has evolved the same degree toward equilibrium and involve the same membrane, the cut-off and resolution are clearly lower for the smaller geometry. This occurs because as the wells become smaller, the transfer time across the membrane becomes a more significant fraction of the diffusion through the entire system, and thus the membrane has a greater resistance relative to the bulk resistance. The 50 μm separation is of particular interest because this form factor could be realized in the development of microfluidic separation devices or bioreactors.

The results above should help guide the design of devices and conditions that achieve separations by diffusion through ultrathin membranes. In comparison to conventional thick membranes,

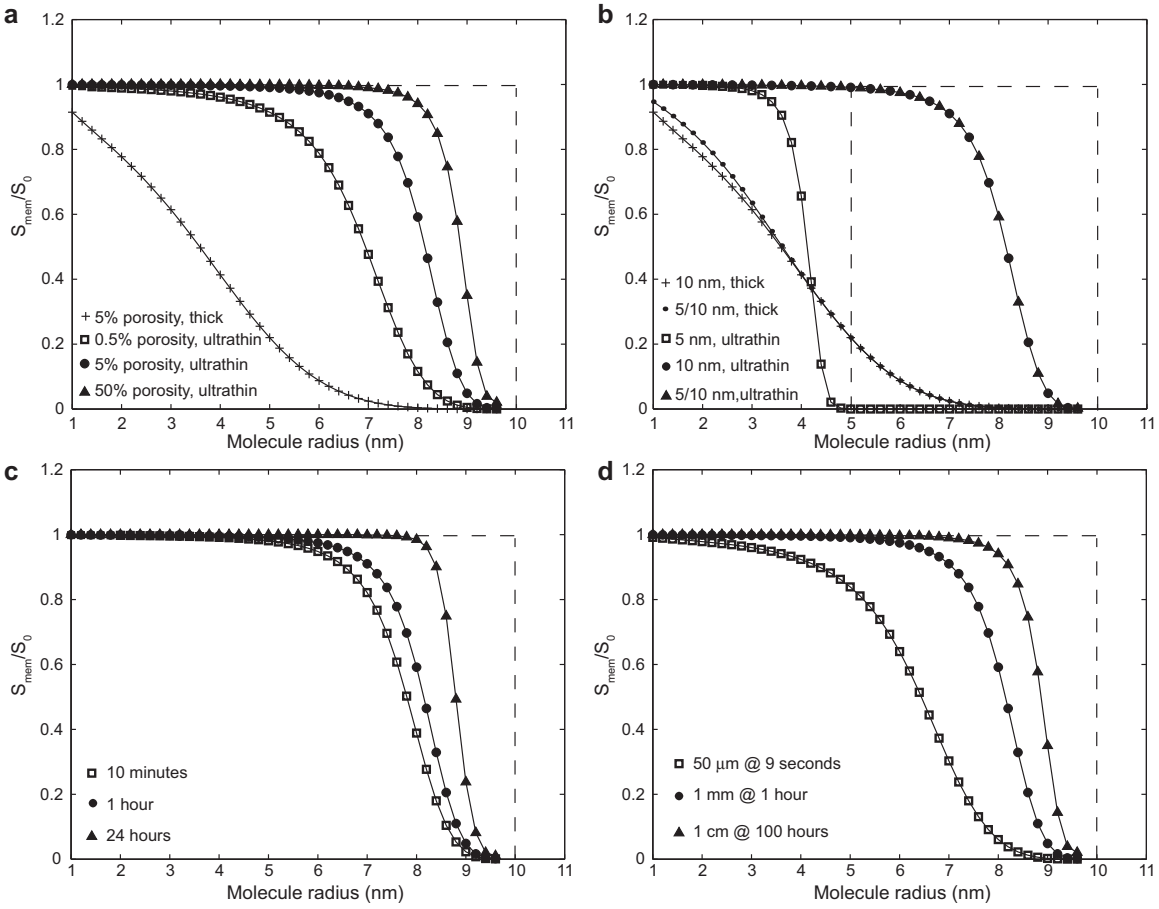

Fig. 7. Factors that influence separations by ultrathin membranes. Here we plot sieving coefficients normalized to sieving coefficients obtain from a membraneless separation (free diffusion case), S_{mem}/S_0, for a series of molecule sizes. This normalized sieving profile shows the extent to which hindrance by the membrane influences the separations. Except for the particular factor being adjusted, the separations are for a 15 nm thick membrane with 5% porosity and 10 nm radius pores for a 1 h separation in a system with 1 mm fluid wells. The dotted line represents equilibrium (time >100 days). (a) Lowering porosity increases the influence of the membrane on molecules below the 10 nm cutoff. A 5 μm thick membrane is included for comparison. (b) Small pores do not change the normalized sieving profile for 15 nm thick membranes. Adding more small pores to a thick membrane has some effect on the sieving profile. Separations with thin membranes are thus governed by the pores close to the physical pore cutoff, while the entire distribution of the membrane affects the separations for thick membrane. (c) The membrane has a greater affect on the normalized sieving profile at shorter time scales. This occurs because slight hindrance differences are significant at short times (d) Smaller wells reach equilibrium faster but are more sensitive to the membrane. Profiles are shown in each case at a characteristic time to equilibrium 0.4τ, where $\tau = a^2/D_0$.

ultrathin membranes will reach equilibrium faster and will enable higher resolution separations at time points far from equilibrium. As separations are carried out for longer times, the resolution of the separation will improve and the molecular cutoff will occur at a size similar to the largest pore size. The yield and purity of the both retentate and dialysate species will also improve with time. At times far from equilibrium, the resolution of separations with ultrathin membranes remains high but has a smaller effective cutoff than suggested by the largest pore size in the distribution. Thus there is an opportunity to purify species well below the absolute cutoff, although with lower yield than a near-equilibrium process would have such short duration separations will require simulations to anticipate the cutoff, resolution, purity, and yield. One important determinant of the quality of separation is the geometry of the diffusion chamber. While smaller volumes approach equilibrium quicker, the contribution of membrane resistance to the total system resistance also becomes higher, and thus benefits smaller systems do not increase in direct proportion to their reduced size.

4.6. Comparison to experiments

Simulations with the 3-D model reveal a high sensitivity to system geometry. A slice through the 3-D model after 10 h of diffusion of a 5 nm radius molecule shows significant depletion directly above the membrane windows but shallow gradients elsewhere, illustrating slow lateral diffusion in the bulk (Fig. 8). Thus the timescale for lateral diffusion in the bulk is a major determinant of the time to equilibrium because of the limited degree to which the membranes span the cross section of the chambers (See Fig. 2).

In Fig. 9, we compare 3-D simulations to diffusion experiments at 24 and 48 h. At both time points, the experimental separations follow the sieving profile predicted from the pore distribution shown in Fig. 1c for all but the largest molecules, β-galactosidase and phophorylase b (Fig. 9a). These results support the prediction that an ultrathin membrane offers effectively no resistance to small molecules but indicates a greater hindrance than predicted by existing sieving models for molecules larger than 30% of the membrane pore size. Note that the retentate and dialysate samples were completely homogenized during collection, and we compare simulations to experiments by integrating the simulated retentate and dialysate wells to compute average concentrations.

There are several likely explanations for the differences between experiments and theory for large molecules. First we note that any factor that reduces measured pore sizes from those measured in TEM micrographs would slow diffusion relative to predictions. For example, electrostatic repulsion would reduce the effective pore size and increase the transmembrane resistance [32,33]. Pre-

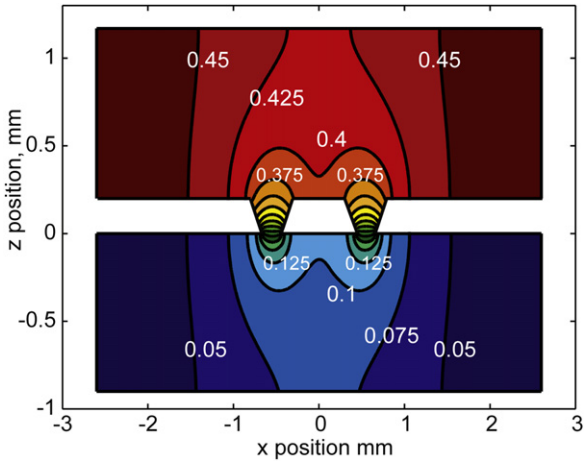

Fig. 8. Slice through 3-D model after 10 h of diffusion of a 5 nm radius molecule. Concentration isolines show diffusion through the membrane (at *z* position 0) from the retentate (top) to the dialysate (bottom).

vious experiments with different salt concentrations have shown that electrostatics do influence the diffusion of molecules through the pores [16]. At the salt concentrations in these experiments (100 mM), the Debye length, or distance to 1/e dropoff of surface potential, is only ~1 nm and so the effect on pore size reduction appears too small to account for the hindrance seen. A rigorous treatment of electrostatics, such as the analysis by Smith and Deen [34], could be used to create more detailed future models in cases where electrostatic interactions are important.

A second known factor that will reduce pore sizes is protein adsorption to the edges of pores. While adsorption causes negligible sample loss to the membrane (Section 4.1), this does not mean that adsorption does not occur. Indeed, we have previously shown that incubation with albumin creates a ~3.5 nm thick protein layer on the internal surface of the pore [16], which is consistent with the thickness of an albumin monolayer [35]. The effects of adsorption can be added to the simulation by subtracting the thickness of the adsorption layer from the pore sizes. We simulated several thicknesses of protein coating, and found that a 5 nm layer fit both the 24 h and the 48 h data (Fig. 9). A 5 nm layer does not impede the diffusion of small molecules, but creates more hindrance for larger molecules. Given that there are several proteins in the system with sizes greater than 5 nm, it is reasonable that a ring of denatured proteins of this size is created within pores. Note that the size and composition of this protein layer may change with time [35].

Another source of potential inaccuracy in our simulations could be found in the hindrance function itself (Eq. (20)). While the theoretical treatments behind this equation establish its validity for $0 \leq \xi \leq 0.95$, few experiments test hindrance theory for molecules close in size to the pore sizes in cylindrical pores [25]. One practical difficulty with verifying the equations for larger particles has been that the passage through long pores is so slow that it is difficult to measure. In this way ultrathin membranes provide an opportunity to test long-standing theories about sieving through cylindrical pores. Proteins are not an ideal choice for such tests, as the effects of protein adsorption, shape, and flexibility contribute complexity (see Supplement for more comprehensive data on molecular shapes and sizes). Future tests of these sieving models should be done with rigid nanoparticles with a known charge density.

The influence of convection is considered to be minimal due to the low volumes and isolation of the system from thermal gradients and air currents, through gravity and osmosis may cause flow through the membrane. Given a 1 mm pressure head, gravity induced flow through the membrane is at best several nanoliters (see Supplement). While collected volumes in rentenate and dialysate are similar to initially pipetted volumes, osmotic pressure calculations indicate that initial volumetric flow rates could fall between 10^{-5} and 10^{-4} μL/s, and could lead to the transfer of ~2 μL (10% volume change) in an hour at the most (see Supplement). The initial flow rate would decrease over time and may be much lower than calculated as the calculation neglected proteins that can pass through the membrane and the highly mobile ions in the buffer. Fluid entering the retentate by osmosis will slow diffusion to the dialysate due to the convection and reduction of the concentration gradient. Experiments with pure proteins at 1 mg/mL and proteins at a partial concentration of 1 mg/mL within a 5 mg/mL mixture have yielded similar sieving coefficients, indicating that effects of osmosis in the more concentrated mixtures are minimal.

Interactions between molecules within the pores, a function of the concentration, might also lead to a discrepancy between experiment and theory. However, total protein mixture concentrations are low enough that molecular interactions would not be predicted in the bulk (see Supplement). Interactions between molecules within pores should also be minimal in ultrathin membranes where pore lengths are similar to molecule sizes, as pores are likely to contain only one molecule at a time.

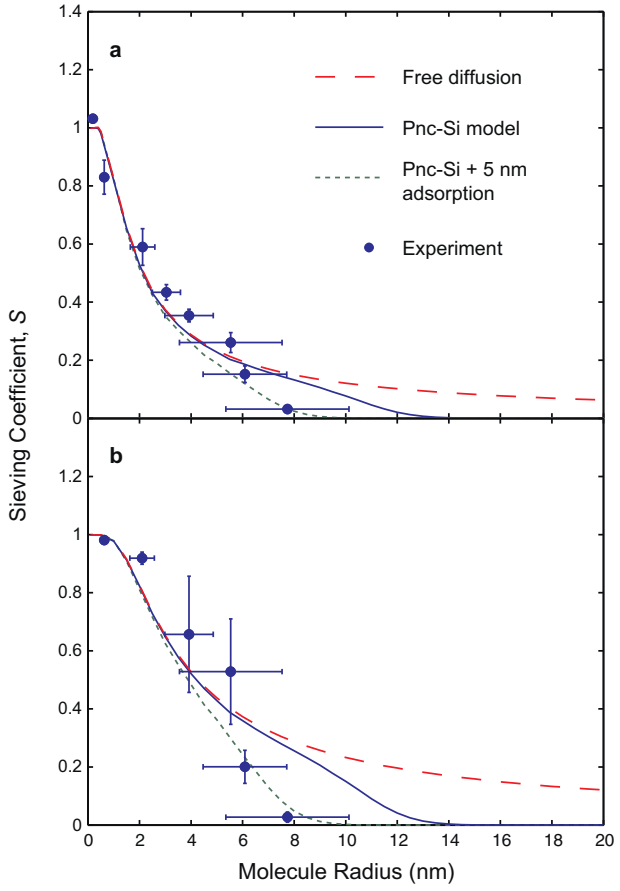

Fig. 9. Experimental and 3-D model sieving profiles for pnc-Si separations at (a) 24 h and (b) 48 h using DLS sizing for experimental data. The sieving profile (solid line) deviates from free diffusion (dashed line) near the physical pore size cutoff. The largest molecules deviate from the theoretical sieving profile. We plot at additional simulation with an added 5 nm protein adsorption ring to the pores, and this adjustment fits the data for both 24 and 48 h.

5. Conclusions

In this work we have performed experimental molecular separations using ultrathin (15 nm) nanoporous membranes and compared experiments to hindrance theory. Ultrathin membranes present a unique opportunity for high resolution separations not afforded by thick conventional membranes. Our 1-D diffusion model indicates that longer times provide higher resolution separations, and ultrathin membranes allow separations to reach equilibrium more quickly than their thicker counterparts. Even far from equilibrium, high resolution separations are attainable with ultrathin membranes. In simulated separations with ultrathin membranes, molecules 30% smaller than the largest membrane pores experience essentially no resistance from the membrane and diffuse as if by free diffusion through the barrier. This contrasts to simulations with 5 μm thick membranes which show hindrance and low resolution at all molecule sizes until very long times. A 3-D model that captures the physical geometry of our experimental system compares well to experimental separations. In our experiments, small molecules and small proteins diffuse through the membrane as if by free diffusion, but the largest proteins exhibit lower sieving coefficients than our model predicts suggesting that neglected factors, such as shape, electrostatics, and adsorption can affect the separation characteristics for larger molecules. The discrepancy between theory and experiments is eliminated if we assume a 5 nm absorbed protein layer reduces all pore sizes identified in the membrane histogram. We expect that the models presented here will help guide the design of experiments and devices that use ultrathin membranes for dialysis and molecular separations, although more advanced sieving models will need to be developed and tested to accurately predict the rate of passage of molecules close in size to the largest pores.

Acknowledgements

The authors would like to acknowledge funding from the National Institutes of Health (R21EB006149) and the National Science Foundation (DMR0722653). The authors would like to thank B. Nehilla for useful discussions and J. DesOrmeaux for fabrication assistance. As founders of SiMPore Inc., TRG, CCS, PMF, and JLM declare a competing financial interest in this work.

Appendix A.

We can solve the problem in Eq. (9) using separation of variables so that

$$\hat{c}(\hat{x},\hat{t}) = \psi(\hat{x})T(\hat{t}). \tag{A.1}$$

The solution for the temporal component of the concentration, $T(t)$, is

$$T(\hat{t}) = e^{-\lambda^2\hat{t}}, \tag{A.2}$$

where λ is a constant. By utilizing the no-flux boundary conditions, Eq. (11), we can obtain the following statement for $\psi(x)$

$$\psi(\hat{x}) = \begin{cases} A_L \cos\lambda\hat{x}, & 0 \le \hat{x} < 1, \\ A_R \cos\lambda(2-\hat{x}), & 1 < \hat{x} \le 2, \end{cases} \tag{A.3}$$

where A_L and A_R are all constants. Flux continuity, Eq. (13), requires

$$(A_L + A_R)\sin\lambda = 0, \tag{A.4}$$

and the concentration jump condition, Eq. (12), allows us to write

$$(A_L - A_R)\cos\lambda = -\beta A_L \lambda \sin\lambda. \tag{A.5}$$

These equations will results in two families of eigenfunctions. The first family is obtained when sin λ in Eq. (A.4) is equal to zero. This set of even eigenfunctions have eigenvalues that are integer multiples of π, so that

$$\lambda_n^{(e)} = n\pi, \quad \psi_n^{(e)} = \cos(n\pi\hat{x}), \quad 0 \le \hat{x} \le 2. \tag{A.6}$$

The second family results when sin λ does not equal zero and instead A_L equals $-A_R$ in Eq. (A.4). In this case Eq. (A.5) reduces to

$$\tan\lambda_n^{(o)} = \frac{2}{\beta\lambda_n^{(o)}}. \tag{A.7}$$

This transcendental equation can be solved to find an infinite number of odd eigenvalues $\lambda_n^{(o)}$ for

$$\psi_n^{(o)} = \begin{cases} \cos\lambda_n^{(o)}\hat{x}, & 0 \le \hat{x} < 1, \\ -\cos\lambda_n^{(o)}(2-\hat{x}), & 1 < \hat{x} \le 2. \end{cases} \tag{A.8}$$

The complete solution of the equation is an eigenfunction expansion of the form

$$\hat{c}(\hat{x},\hat{t}) = c_o + \sum_{n=1}^{\infty} c_n \psi_n(\hat{x}) e^{-\lambda_n^2\hat{t}}, \tag{A.9}$$

where the coefficients c_o and c_n are solved for using the initial value, Eq. (14), and the following relations:

$$c_0 = \frac{1}{2}\int_0^2 \hat{c}(\hat{x},0)\,d\hat{x}, \tag{A.10}$$

$$c_n = \frac{\int_0^2 \hat{c}(\hat{x},0)\psi(\hat{x})\,d\hat{x}}{\int_0^2 \psi^2(\hat{x})\,d\hat{x}}. \tag{A.11}$$

Thus the final solution is

$$\hat{c}(\hat{x},\hat{t}) = \frac{1}{2} + \sum_{n=1}^{\infty} \frac{\sin\lambda_n}{\lambda_n + \cos\lambda_n \sin\lambda_n} \psi_n(\hat{x}) e^{-\lambda_n^2\hat{t}}. \tag{A.12}$$

It should be noted that all even eigenfunctions, other than the one associated with $\lambda_0^{(e)}$, give zero coefficients. This means that Eq. (A.12) requires the odd eigenfunctions given by Eq. (A.7) and only the constant first even eigenfunction, c_0.

Appendix B.

An additional 1-D analytical model lacking a membrane, or the free diffusion case, was simulated for comparison purposes. The following problem was scaled using Eq. (9) in the text:

$$\frac{\partial\hat{c}}{\partial\hat{t}} = \frac{\partial^2\hat{c}}{\partial\hat{x}^2}, \quad 0 \le \hat{x} \le 2, \tag{B.1}$$

$$\frac{\partial\hat{c}}{\partial\hat{x}}(0,\hat{t}) = 0, \quad \frac{\partial\hat{c}}{\partial\hat{x}}(2,\hat{t}) = 0, \tag{B.2}$$

$$\hat{c}(\hat{x},0) = \begin{cases} 1, & 0 \le \hat{x} < 1, \\ 0, & 1 < \hat{x} \le 2, \end{cases} \tag{B.3}$$

where Eq. (B.1) is Fick's Second Law of Diffusion, (B.2) the no flux conditions, and (B.3) the initial value. The solution to this problem is:

$$\hat{c}(\hat{x},\hat{t}) = \frac{1}{2} + \sum_{n=1}^{\infty} \frac{\sin\lambda_n}{\lambda_n} \cos(\lambda_n\hat{x}) e^{-\lambda_n^2\hat{t}}, \tag{B.4}$$

where

$$\lambda_n = \frac{n\pi}{2}. \tag{B.5}$$

Nomenclature

A	area of TEM image (m^2)
a	length of fluid well (m)
c	solute concentration (mol/L)
$\hat{c}$	non-dimensional concentration
D	diffusion coefficient (m^2/s)
D_0	free diffusion coefficient (m^2/s)
D_m	membrane diffusion coefficient (m^2/s)
d	membrane thickness (m)
F_m	flux within the membrane ($mol\,m^{-2}\,s^{-1}$)
F_f	flux within the fluid wells ($mol\,m^{-2}\,s^{-1}$)
k	Boltzmann's constant ($m^2\,kg\,s^2\,K^{-1}$)
N	pore density (number/m^2)
n	an integer
P_d	pore discovery permeability (m/s)
P_t	transmembrane permeability (m/s)
R_p	pore radius (m)
R_s	molecule radius (m)
S	sieving coefficient
t	time (s)
$\hat{t}$	non-dimensional time
x	position (m)
$\hat{x}$	non-dimensional position

Greek letters

β	resistance parameter
η	viscosity (Pa s)
κ	permeability (m/s)
λ_n	eigenvalues
ξ	R_s/R_p
τ	characteristic time (s)
ψ_n	eigenfunctions
Ω_m	membrane resistance (s/m)
Ω_w	well resistance (s/m)

Appendix C. Supplementary Data

Supplementary data associated with this article can be found, in the online version, at doi:10.1016/j.memsci.2010.11.056.

References

[1] M.D. Luque de Castro, F. Priego Capote, N. Sánchez Ávila, Is dialysis alive as a membrane-based separations technique? TrAC, Trends Anal. Chem. 27 (2008) 315.
[2] W.H. Fissell, H.D. Humes, A.J. Fleischman, S. Roy, Dialysis and nanotechnology: now, 10 years, or never? Blood Purif 25 (2007) 12.
[3] S. Mochizuki, A.L. Zydney, Theoretical analysis of pore size distribution effects on membrane transport, J. Mem. Sci. 82 (1993) 211.
[4] R. Vanholder, G. Glorieux, W. Van, Biesen, Advantages of new hemodialysis membranes and equipment, Nephron Clin. Pract. 114 (2010) c165.
[5] M. Jadoul, Dialysis-related amyloidosis: importance of biocompatibility and age, Nephrol. Dial. Transpl. 13 (1998) 61.
[6] A.K. Cheung, M.V. Rocco, G. Yan, J.K. Leypoldt, N.W. Levin, T. Greene, L. Agodoa, J. Bailey, G.J. Beck, W. Clark, A.S. Levey, D.B. Ornt, G. Schulman, S. Schwab, B. Teehan, G. Eknoyan, Serum, β-2 microglobulin levels predict mortality i dialysis patients: results of the HEMO study, J. Am. Soc. Nephrol. 17 (2006) 546.
[7] D. Lee, M. Haase, A. Hasse-Fielitz, K. Paizis, H. Goehl, R. Bellomo, A pilot, randomized, double-blind, cross-over study of high cut-off versus high-flux dialysis membranes, Blood Purif. 28 (2009) 365.
[8] D.H. Krieter, B. Canaud, High permeability of dialysis membranes: what is the limit of albumin loss, Nephrol. Dial. Transplant. 18 (2003) 651.
[9] J.P. Kooman, F.M. van der Sande, K.M. Leunissen, The long road to wearable blood-cleansing devices, Blood Purif. 25 (2007) 377.
[10] W.H. Fissell, A. Dubnisheva, A.N. Eldridge, A.J. Fleishman, A.L. Zydney, S. Roy, High-performance silicon nanopore hemofiltration membranes, J. Mem. Sci. 326 (2009) 58.
[11] C.A. Lopez, A.J. Fleischamn, S. Roy, T.A. Desai, Evaluation of silicon nanoporous membranes and ECM-based microenvironments on neurosecretory cells, Biomaterials 27 (2006) 3075.
[12] J.K. Holt, H.G. Park, Y. Wang, M. Stadermann, A.B. Artyukhin, C.P. Grigoropoulos, A. Noy, O. Bakajin, Fast mass transport through sub-2-nanometer carbon nanotubes, Science 312 (2006) 1034.
[13] B.J. Hinds, N. Chopra, T. Rantell, R. Andrews, V. Gavalas, L.G. Bachas, Aligned multiwalled carbon nanotube membranes, Science 303 (2004) 62.
[14] H.D. Tong, H.V. Jansen, V.J. Gadgil, C.G. Bostan, E. Berenschot, C.J.M. van Rijn, M. Elwenspoek, Silicon nitride nanosieve membrane, Nano Lett. 4 (2004) 283.
[15] H.U. Osmanbeyoglu, T.B. Hur, H.K. Kim, Thin alumina nanoporous membranes for similar size biomolecule separation, J. Mem. Sci. 343 (2009) 1.
[16] C.C. Striemer, T.R. Gaborski, J.L. McGrath, P.M. Fauchet, Charge- and size-based separation of macromolecules using ultrathin silicon membranes, Nature 445 (2007) 749.
[17] E. Kim, H. Xiong, C.C. Striemer, D.Z. Fang, P.M. Fauchet, J.L. McGrath, S. Amemiya, A structure-permeability relationship of ultrathin nanoporous silicon membrane: a comparison with the nuclear envelope, J. Am. Chem. Soc. 130 (2008) 4230.
[18] T.R. Gaborski, J.L. Snyder, C.C. Striemer, D.Z. Fang, M. Hoffman, P.M. Fauchet, J.L. McGrath, High performance separation of nanoparticles with ultrathin porous nanocrystalline silicon membranes, ACS Nano 4 (2010) 6973.
[19] A.A. Agrawal, B.J. Nehilla, K.V. Reisig, T.R. Gaborski, D.Z. Fang, C.C. Striemer, P.M. Fauchet, J.L. McGrath, Porous nanocrystalline silicon membranes as highly permeable and molecularly thin substrates for cell culture, Biomaterials 31 (2010) 5408.
[20] E.M. Renkin, Filtration, diffusion, and molecular sieving through porous cellulose membranes, J. Gen. Physiol. 38 (1954) 225.
[21] R.E. Beck, J.S. Schultz, Hindered diffusion in microporous membranes with known pore geometry, Science 170 (1970) 1302.
[22] S.K. Dalvie, R.E. Baltus, Transport studies with porous alumina membranes, J. Mem. Sci. 71 (1992) 247.
[23] P.M. Bungay, H. Brenner, The motion of a closely-fitting sphere in a fluid-filled tube, Int. J. Multiphase Flow 1 (1973) 25.
[24] W.M. Deen, Hindered transport of large molecules in liquid-filled pores, AlChE J. 33 (1987) 1409.
[25] P. Dechadilok, W.M. Deen, Hindrance factors for diffusion and convection in pores, Ind. Eng. Chem. Res. 45 (2006) 6953.
[26] A.M. Berezhkovskii, Y.A. Makhnovskii, M.I. Monine, V.Y. Zitserman, S.Y. Shvartsman, Boundary homogenization for trapping by patchy surfaces, J. Chem. Phys. 121 (2004) 21.
[27] H.C. Berg, Random Walks in Biology, Princeton University Press, Princeton, NJ, USA, 1993.
[28] T.F. Weiss, Cellular Biophysics, vol. 1, Transport, MIT Press, Cambridge, MA, USA, 1996.
[29] Y.A. Makhvovskii, A.M. Berezhkovskii, V.Y. Zitserman, Homogenization of boundary conditions on surfaces randomly covered by patches of different sizes and shapes, J. Chem. Phys. 122 (2005) 236102.
[30] D.R. Latulippe, K. Ager, A.L. Zydney, Flux-dependent transmission of supercoiled plasmid DNA through ultrafiltration membranes, J. Mem. Sci 294 (2007) 169.
[31] Rasband, W.S., Image J, U.S. National Institutes of Health, Bethesda, Maryland, USA. http://rsb.info.nih.gov/ij/, 1997.
[32] N.S. Pujar, A.L. Zydney, Electrostatic and electrokinetic interactions during protein transport through narrow pore membranes, Ind. Eng. Chem. Res. 33 (1994) 2473.
[33] W.D. Munch, L.P. Zestar, J.L. Anderson, Rejection of polyelectrolytes from microporous membranes, J. Mem. Sci. 5 (1979) 77.
[34] F.G. Smith, W.M. Deen III, Electrostatic effects on the partitioning of spherical colloids between dilute bulk solution and cylindrical pores, J. Colloid Interf. Sci. 91 (1983) 571.
[35] M.S. Ehrenberg, A.E. Friedman, J.N. Finkelstein, G. Oberdorster, J.L. McGrath, The influence of protein adsorption on nanoparticle association with cultured endothelial cells, Biomaterials 30 (2009) 603.